International Journal of Radiation Oncology biology • physics

www.redjournal.org

Physics Contribution

Simulation Model of Microsphere Distribution for Selective Internal Radiation Therapy Agrees With Observations

Jonas Högberg, PhD,* Magnus Rizell, MD, PhD,† Ragnar Hultborn, MD, PhD,‡ Johanna Svensson, MD, PhD,‡ Olof Henrikson, MD,§ Johan Mölne, MD, PhD,‖ Peter Gjertsson, MD, PhD,¶ and Peter Bernhardt, PhD*,#

**Department of Radiation Physics, Sahlgrenska Academy, University of Gothenburg, Gothenburg, Sweden; and Departments of †Surgery, ‡Oncology, §Radiology, ‖Pathology, ¶Clinical Physiology, and #Medical Physics and Biomedical Engineering, Sahlgrenska University Hospital, Gothenburg, Sweden*

Received Dec 3, 2015, and in revised form Apr 19, 2016. Accepted for publication May 5, 2016.

Summary

Microsphere clusters are common in normal liver tissue arteries after radioembolization. To describe microsphere-clustering properties, we analyzed the microsphere distribution in patient biopsies and constructed a hepatic artery branching tree model that successively branched into 2 new generations of arteries at 20 nodes. In agreement with the clinical findings, simulations revealed that microsphere clusters are larger and more common in volumes with high microsphere concentrations than has been previously predicted.

Purpose: To perform a detailed analysis of microsphere distribution in biopsy material from a patient treated with ^{90}Y-labeled resin spheres and characterize microsphere distribution in the hepatic artery tree, and to construct a novel dichotomous bifurcation model for microsphere deposits and evaluate its accuracy in simulating the observed microsphere deposits.

Methods and Materials: Our virtual model consisted of arteries that successively branched into 2 new generations of arteries at 20 nodes. The artery diameter exponentially decreased from the lowest generation to the highest generation. Three variable parameters were optimized to obtain concordance between simulations and measure microsphere distributions: an artery coefficient of variation (ACV) for the diameter of all artery generations and the microsphere flow distribution at the nodes; a hepatic tree distribution volume (HDV) for the artery tree; and an artery diameter reduction (ADR) parameter. The model was tested against previously measured activity concentrations in 84 biopsies from the liver of 1 patient. In 16 of 84 biopsies, the microsphere distribution regarding cluster size and localization in the artery tree was determined via light microscopy of 30-µm sections (mean concentration, 14 microspheres/mg; distributions divided into 3 groups with mean microsphere concentrations of 4.6, 14, and 28 microspheres/mg).

Results: Single spheres and small clusters were observed in terminal arterioles, whereas large clusters, up to 450 microspheres, were observed in larger arterioles. For 14 microspheres/mg, the optimized parameter values were ACV = 0.35, HDV = 50 cm^3, and

Reprint requests to: Jonas Högberg, PhD, Department of Radiation Physics, Sahlgrenska Academy, University of Gothenburg, Gula stråket 2B, SE-41346 Gothenburg, Sweden. Tel: (+46) (0) 736254123; E-mail: jonas.hogberg@radfys.gu.se

This work was financially supported by the Swedish Cancer Society, Swedish Radiation Safety Authority, and the King Gustav V Jubilee Clinic Cancer Research Foundation.

Conflict of interest: none.

Int J Radiation Oncol Biol Phys, Vol. 96, No. 2, pp. 414–421, 2016

http://dx.doi.org/10.1016/j.ijrobp.2016.05.007

ADR = 6 μm. For 4.6 microspheres/mg, ACV and ADR decreased to 0.26 and 0 μm, respectively, whereas HDV increased to 130 cm^3. The opposite trend was observed for 28 microspheres/mg: ACV = 0.49, HDV = 20 cm^3, and ADR = 8 μm.
Conclusion: Simulations and measurements reveal that microsphere clusters are larger and more common in volumes with high microsphere concentrations and indicate that the spatial distribution of the artery tree must be considered in estimates of microsphere distributions.

Introduction

In radioembolization, ^{90}Y-labeled microspheres are selectively infused into the hepatic artery system and lodged into tumors and in the hepatic parenchyma at a lower concentration because of its low support of arterial blood. With this treatment modality, tumor reduction can be achieved with minor radiation-induced hepatic damage (1, 2). Of interest, the tolerated mean absorbed dose of the normal liver parenchyma is considerably higher than for external beam irradiation (2). The most probable main factor in the high radiation tolerance of the parenchyma is the nonuniform distribution of microspheres (3), but this role has not been fully verified by descriptive modeling because of the lack of detailed microsphere distributions in human livers.

In a limited number of studies, however, the high variability in normal human parenchyma has been described by detector measurement and light microscopy investigations of liver biopsies. Using detector measurements, Burton et al (4) investigated 16 biopsies, 0.6 to 10 g each and cut into 0.1- to 0.2-g samples, and found high variability. The mean absorbed biopsy doses were 9 to 75 Gy, and the coefficient of variation (CV) for each biopsy ranged between 22% and 160%. Similar results also have been obtained with smaller biopsy samples (0.08-0.4 g) and with autoradiography of thin-sliced normal liver tissues (dimensions 0.02 × 4 × 6 cm) (5, 6). Light microscopy analysis of thin-sliced (8-10 μm) normal parenchyma biopsies has been performed (7-9), showing that multiple microspheres can be gathered in arterioles; however, the distances between the analyzed sections were 0.2 to 0.5 mm, and the total cluster size through serial sections was therefore not described. In one recent study, though, serial sections of 30 μm were investigated (6), showing that clusters of several hundred microspheres can be generated in larger arterioles in the artery tree. Nonetheless, knowledge is still lacking regarding the distribution of clusters and their location in different-sized arterioles.

Recently, Walrand et al (3) presented an artery branching tree model to explain the gathering of clusters and the higher tolerance to radiation of normal liver parenchyma after radioembolization of liver tumors; this study contrasted glass microspheres (Theraspheres) with resin microspheres (SIR-Spheres; Sirtex Medical Limited, North Sydney, Australia) used in selective internal radiation therapy (SIRT). In glass microsphere–based treatments, the activity per microsphere is 50 times higher (2500 Bq per microsphere) than in treatments with resin microspheres (50 Bq per microsphere). Consequently, the number of microspheres injected for a given absorbed dose is less for glass microspheres (10, 11). By introducing uneven microsphere distribution probabilities throughout the branches in the arterial tree, Walrand et al (3) revealed that glass microspheres cause nonuniformities in the microsphere distribution, with some final terminal arterioles in the portal tracts lacking microspheres, some containing single microspheres, and some with smaller clusters. Walrand et al (3) assumed that all microspheres ended up in the final terminal arterioles in the portal tracts, without considering clustering in the larger arterioles. Their corresponding simulations of the distribution of resin microspheres (ie, increasing the total number of microspheres) yielded a much more uniform distribution of the absorbed dose than that obtained from simulations of glass microspheres (1). However, Högberg et al (6) showed that large microsphere clusters commonly occur in larger normal liver tissue arteries after radioembolization with resin microspheres; this treatment resulted in a less uniform absorbed dose distribution for resin microspheres than that predicted by direct application of the model of Walrand et al (3).

Recently Debbaut et al (12) analyzed the architecture of human liver vasculature by combining vascular corrosion casting and x-ray microtomography. These authors found that artery diameters decreased exponentially with increasing artery generation number. The CV of vessel diameter ranged from 0.13 to 0.21 across vessel generations, resulting in considerable variation in artery architecture and thus in the potential for variation in circulatory characteristics within artery generations (12). Furthermore, Debbaut et al (12) demonstrated that the branching pattern of the artery tree is highly variable and that a dichotomous bifurcation model in which a parent artery is divided into 2 daughter arteries is an overly simplified version of a native hepatic artery tree. In fact, the estimated number of arteries in human livers is 100-fold higher than the number of arteries in a dichotomous bifurcation model because of parent artery division into 3 or more daughter arteries and the existence of small side branches that are almost perpendicular to the parent artery (12). In addition, the terminal ending of the artery tree is a complex structure, in contrast

to the portal vein system where the terminal portal veins straightforwardly continue with the sinusoids into the hepatic lobule. The terminal arterioles, meanwhile, diverge into different portal tract structures such as the portal veins, bile ducts, sinusoids, and connective tissue in the portal tract for delivering oxygen-enriched blood (13). Because of its complexity, the total human hepatic artery architecture is thus far not fully described (13-18). Nevertheless, advanced bifurcation modeling of the hepatic vessel tree has revealed good matching with the main structure of the vessel tree and might therefore be accurate enough for modeling of the microsphere transport (19).

In this study we performed a detailed analysis of the microsphere distribution in biopsy material from a patient treated with ^{90}Y-labeled resin spheres (5, 6) and characterized the microsphere distribution in the hepatic artery tree. Furthermore, we constructed a novel dichotomous bifurcation model for microsphere deposits and evaluated its accuracy in simulating the observed microsphere deposits.

Methods and Materials

Patient and clinical procedures

All procedures performed in studies involving human participants were approved by the Regional Ethical Review Board in Gothenburg, Sweden, and were in accordance with the 1964 Helsinki declaration and its later amendments or comparable ethical standards. We compared simulations with previous investigations of microsphere distributions in 3 patients. In this work we extended earlier analysis by measuring vessel diameters at the sites of microsphere clustering in 1 patient. The procedure was recently described by Högberg et al (5-7). Briefly, a female, aged 62 years, suffered from a marginally resectable cholangiocarcinoma and agreed to undergo neoadjuvant treatment with ^{90}Y-labeled microspheres (SIRT) followed by liver surgery. The patient was first examined via selective hepatic artery angiography and artery coiling, followed by injection with ^{99m}Tc-labeled macro-aggregated albumin (^{99m}Tc-MAA) for planar imaging and single-photon emission computed tomography/computed tomography to evaluate the hepatic distribution and fraction of pulmonary shunting of ^{99m}Tc-MAA. Two weeks later, the hepatic artery was recannulated for infusion with ^{90}Y-labeled SIR-Spheres. Thirty million microspheres (1.6 GBq) were suspended in 30 to 40 mL distilled water and injected within 1 hour. Nine days later, the patient underwent liver surgery with an ultrasonic cavitron aspirator (tumor resection), including resection of a margin of surrounding normal liver tissue (5, 6, 20).

Microsphere distributions in resected liver tissue

Shortly after resection, the volume of liver and tumor tissue was immersed in isotonic formaldehyde for 48 hours and then machine-sliced into sections 1- to 2-mm thick. Microsphere distribution analysis was conducted via autoradiography, punch-biopsy activity measurements, and light microscopy (5, 6, 20). Punch-biopsy measurements (n = 84) revealed that the CV for the activity concentration decreased with increasing sample size (CVs of 1.4, 1.0, and 0.63 for mean sample sizes of 10 mg, 27 mg, and 66 mg, respectively) (5). Light microscopy was used to investigate the frequency of single microspheres and microsphere clusters in arterioles and small arteries in 15 sequential sections 30-μm thick from 16 punch biopsies of normal liver parenchyma (each biopsy 6-8 mm in diameter) (6). To obtain 15 sequential sections from each biopsy, we used biopsies from the largest group (ie, the 66-mg group).

With light microscopy, we measured artery diameters at cluster deposits and divided the clusters into artery generations according to the measured diameter sizes. Biopsies were further categorized into 3 groups depending on microsphere concentration: 4.6 microspheres/mg tissue (n = 5), 14 microspheres/mg tissue (n = 6), and 28 microspheres/mg tissue (n = 5), with standard deviations of 2.0, 4.6, and 4.2, respectively.

Assumptions regarding hepatic artery tree structure

Microsphere transport and distributions were simulated by a hepatic arterial branching tree model, constructed as a dichotomous bifurcation model with the arteries branching into new arteries at 20 nodes to yield 21 generations of arteries. The mean diameters of the various artery generations (g) exponentially decreased with each artery generation, in agreement with Debbaut et al (12):

$$D(g) = 8.4e^{-0.31g} \quad (1)$$

The artery tree then consisted of arteries with a mean diameter of 6.1 mm for the first generation down to a mean diameter of 13 μm for the 21st generation. The probability of entrapment was assumed to depend on diameter size, which was normally distributed between the arteries in a generation (Eq. 3). The magnitude of the diameter variation was set by the artery CV (ACV) parameter. We also assumed that the different microsphere concentrations observed in the 3 groups of biopsies can result from different local ACV, because of different distribution volumes for the arterial tree, as discussed below.

To investigate whether the obtained difference in microsphere concentrations arose from differences in the spatial distribution of the artery tree, we introduced a hepatic tree distribution volume (HDV) parameter (ie, the volume within which the artery tree is distributed). The number of microspheres (n) simulated for a microsphere concentration (MSC) is then determined by:

$$n = \mathrm{MSC} \times \mathrm{HDV} \times d \times 1000 \quad (2)$$

Here the unit of HDV is cm^3, and the density (d) is assumed to be 1. The physical consequences of a reduced HDV are that the artery tree will be compressed and more

tortuous. Consequently, a more tortuous tree might influence microsphere transport and the probability of entrapment. To study this factor, we added an artery diameter reduction (ADR) parameter into the model (ie, a constant reduction of the artery diameter).

In summary, for every artery (i) in each generation, the artery diameter, D_A, which determines the probability of entrapment and the transport through the arterial tree, was randomly determined by:

$$D_A(g,i) = D(g) \times (1 + \mathrm{ACV} \times r) - \mathrm{ADR} \qquad (3)$$

where r is a normally distributed random variable. The D_A was truncated for preventing negative artery diameters.

The simulation starts with creation of all artery diameters (Eq. 3) in the hepatic artery tree. In this hepatic artery tree the transport of the n microspheres (Eq. 2) are followed one by one. The transport starts by random selection of the microsphere diameter, having a mean of 32.5 µm and a CV equal to 0.077 (10). Thereafter the microsphere transports are followed through the different nodes in the artery tree. The path of the microsphere at the nodes was randomly determined by the ratio of the 2 related artery diameters, favoring transport through the largest artery diameter. The microspheres were followed in this way to an entrapment site consisting of an artery generation with a diameter smaller than the microsphere diameter. Such entrapment blocked the transport of subsequent microspheres, possibly resulting in microsphere clustering. In addition, we investigated the influence of the lower artery generation on microsphere entrapment by starting the simulation at different generations in the artery tree.

Parameter values for ACV, ADR, and HDV were determined by iteratively comparing the simulation results with the observed microsphere distributions in human liver biopsies. The ACV values were normally distributed and varied between 0 and 1.00, HDV values varied between 1 and 1500 cm^3, and ADR values varied between 0 and 10 µm.

Results

Light microscopy revealed various forms of liver lobules (Fig. 1A) with microsphere entrapments in arterioles of various sizes (Fig. 1B-D). The often-used schematic representation of the lobule as a symmetric hexagonal form was seldom observed; instead, irregular forms were more common, as has been previously described (13-18). Furthermore, the portal tracts were seldom observed as a portal triad (ie, a portal tract with 1 artery, 1 vein, and 1 bile duct). Instead, various combinations of the 3 units were more frequent, in line with recent findings (14). Figure 1B shows an example of a portal tract with 4 different-sized arterioles, where one is filled with several microspheres. In Figure 1C, a bulky cluster is located at a node site (ie, where the arteriole is divided into 2 smaller arterioles), and in Figure 1D a string of spheres is entrapped in a small arteriole.

Figure 2 shows the cumulative microsphere distributions from 16 biopsies and the simulation results. Cluster deposits mainly occurred in high artery generations. However, the largest clusters were always located in the largest arterioles. For parameter values of ACV = 0.35, HDV = 50 cm^3, and ADR = 6 µm, a good concordance was achieved between simulations and the measured cumulative frequencies of microsphere distributions according to microspheres per cluster or to artery generations, for the 16 biopsies (R^2>0.99; Fig. 2A, B). Good agreement was also obtained with these parameter values for samples of different sizes (Fig. 2C): the CVs for the activity

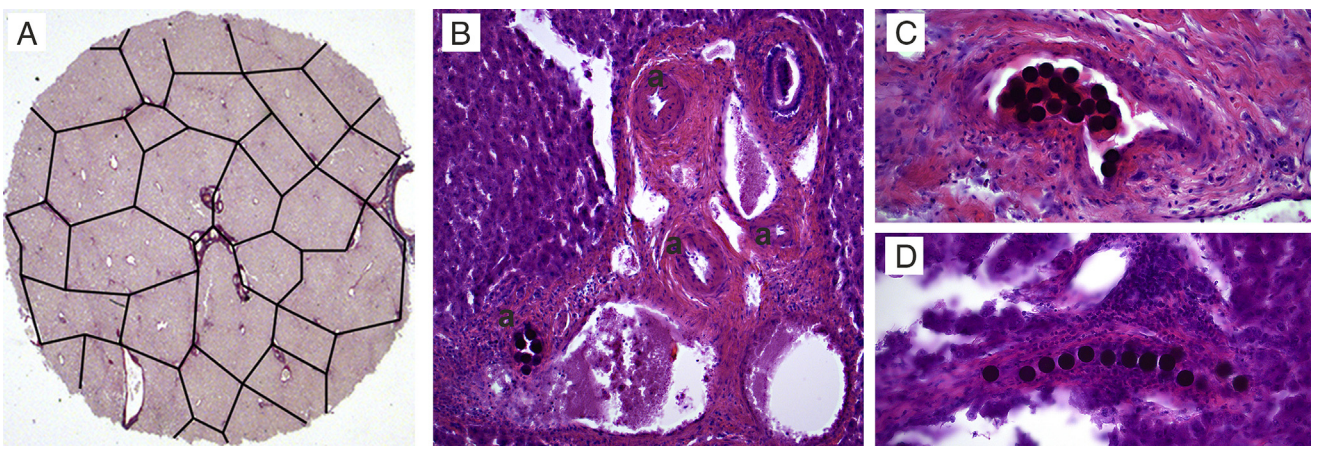

Fig. 1. Liver architecture and microsphere distributions. (A) Punch biopsy (diameter 8 mm) in which the liver lobules were outlined manually. Lobules differ substantially in size and shape. (B-D) Light microscopy of 3 sections (30 µm) with different microsphere-cluster dimensions. (B) A portal tract with 4 arterioles (a) in which the artery cross-section in the left corner is filled with 9 microspheres; these spheres are part of a 122-microsphere cluster. (C) Section of an arteriole that is dividing into 2 smaller arterioles; this section of the node is filled with 24 microspheres. (D) String of 13 microspheres in a horizontal section of an arteriole.

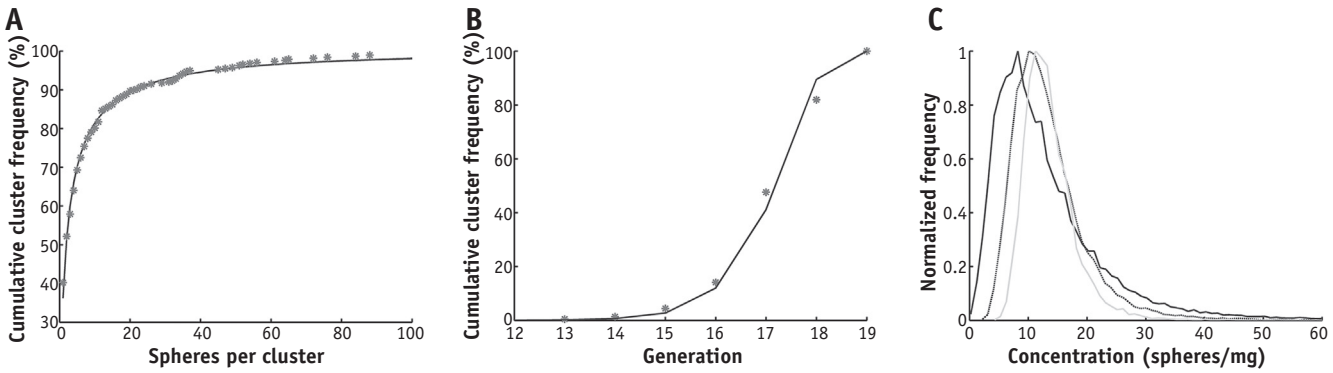

Fig. 2. Comparison of simulations (line) and measured microsphere distributions (dots). (A) Cumulative cluster frequency versus microspheres per cluster (14 microspheres/mg concentration). (B) Cumulative cluster frequency versus artery generation for measured biopsies (dots) and simulation (line) (R^2>0.99; 14 microspheres/mg). (C) Simulations of the distribution of microsphere concentration in 10-mg (black line), 27-mg (black dotted line), and 66-mg (grey line) samples. Note the more normally distributed frequency curves and decreasing coefficients of variation for higher microsphere concentrations.

concentration in the 10-mg, 27-mg, and 66-mg samples were 1.4, 1.0, and 0.56, respectively. The corresponding CVs for punch-biopsy activity measurements, in the work by Högberg et al (5), were 1.4 (n=29), 1.0 (n=26), and 0.63 (n=29), respectively.

Figure 3 depicts the cumulative frequencies of the microsphere distributions for 3 microsphere concentrations and the best fit to simulations (R^2>0.98). In comparison with simulations with the mean microsphere concentration of 14 microspheres/mg, ACV and ADR decreased to 0.26 and 0 μm, respectively, for the lower concentration of 4.6 microspheres/mg, but the HDV increased to 130 cm^3. For 28 microspheres/mg, the opposite result was obtained; the optimal parameter values were ACV=0.49, HDV=20 cm^3, and ADR = 8 μm (Table 1). Of note, a microsphere concentration increase was accompanied by a decrease in HDV of the same magnitude (Table 1).

In both the experimental analyses and the simulation, the microspheres were deposited in generations 12 and upward. The influence of the transport through the first generations was of minor importance because almost identical results were obtained when the simulation started in generations 2 to 9; simulations started at higher generations resulted in deviations from the obtained experimental results.

Discussion

The present study demonstrates that simulations from a dichotomous bifurcation model can agree with microsphere distributions measured in liver samples both regarding cluster size and their deposits in the artery tree. The main histologic distinction among the arteries, arterioles, and terminal arterioles in the hepatic artery tree is the number of

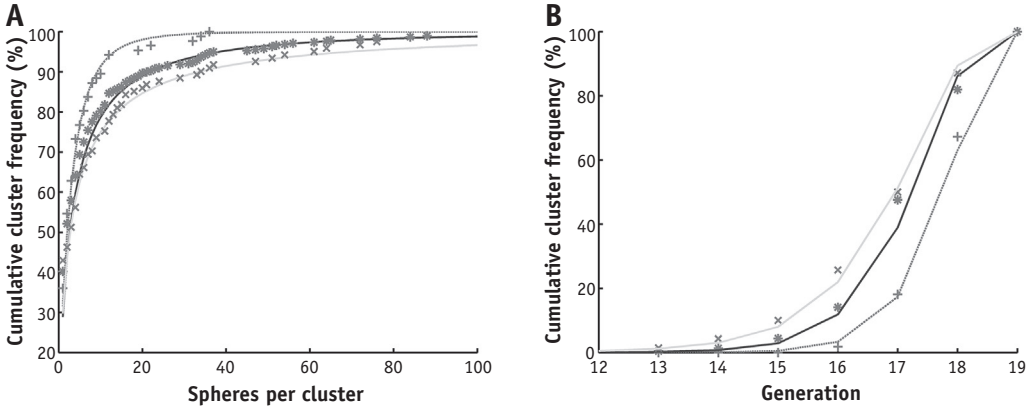

Fig. 3. Cumulative cluster frequency versus microspheres/cluster (A) and artery generation (B) for measured biopsies (dots) and simulations (lines). Simulations of microsphere distributions for different microsphere concentrations yielded different parameter values. The best fits to the mean biopsy microsphere concentrations of 4.6 microspheres/mg (+ and dotted line), 14 microspheres/mg (o and black line), and 28 microspheres/mg (x and grey line) were achieved with artery coefficient of variation values of 0.26, 0.35, and 0.49, respectively; hepatic tree distribution volume values of 130 cm^3, 50 cm^3, and 20 cm^3, respectively; and artery diameter reduction values of 0 μm, 6 μm, and 8 μm, respectively (R^2>0.98).

Table 1 Parameter settings for the different mean biopsy microsphere (MS) concentrations

MS concentration (mg^{-1})	HDV (cm^3)	ACV	ADR (μm)
4.6	130	0.26	0
14	50	0.35	6
28	20	0.49	8

Abbreviations: ACV = artery coefficient of variation; ADR = artery diameter reduction; HDV = hepatic tree distribution volume.

smooth muscle cells around the endothelial cells, where the arteries have more than 3, which is often observed down to an artery diameter of 500 μm (13). In these arteries, no microspheres were found. The arterioles (diameter of approximately 50-500 μm, generations 16 and 9, respectively) consist of 3 to 2 smooth muscle cells, whereas the terminal arterioles have 1 smooth muscle cell (diameter <50 μm). The largest clusters with aggregated strings of microspheres (50-100 microspheres per cluster) and very large, bulky clusters (100-500 microspheres per cluster) were observed in arterioles smaller than 200 μm (generation 12), whereas single microspheres and microsphere strings (<50 microspheres per cluster) were found in the terminal arterioles. However, we could not distinguish microsphere deposits in higher generations (ie, 19-21 [diameters of 23 and 13 μm, respectively]), and consequently these microspheres were summed up in generation 19. With these biopsy cluster discoveries, we showed good agreement with simulations. For a high concentration of microspheres (28 microspheres/mg), our simulations indicated a higher frequency of large clusters than observed in biopsies. It is, however, possible that some large and very large biopsy clusters were truncated because the number of sequential sections was limited to 15 (30 μm thick, 450 μm in total).

In the proposed model, we assumed that microspheres are transported through the hepatic tree until entrapment due to spatial constraints in the vessels. We further assumed that these variations may be described by the ADR and ACV parameters, which inherently include specific factors that influence the entrapment probabilities of the microspheres to various degrees. Debbaut et al (12) reported that artery diameter decreases exponentially, with a mean CV of the diameter of 0.20. In our simulations, ACV was >0.26, indicating that other factors, such as vessel curvature and elasticity (21), could strongly influence microsphere entrapment. Furthermore, our simulations showed that increasing observed microsphere density corresponds to increased ACV, perhaps because of the random trapping process alone. Alternatively, this observation may reflect spatial variations of the artery tree structure in the liver.

Fitting higher microsphere concentration with the model results in a decreased HDV value and in an increased ADR value. The latter of these is used for modeling the increased probability for entrapment of microspheres in a more compressed and tortuous artery tree (21), which would be the consequences of a reduced HDV. However, for an increased number of microspheres, the ADR value might also reflect the increased probability for sphere aggregations during transport through the artery tree. Exclusion of the ADR parameter from the model required an increase in ACV to obtain the best, but inferior, fit to the measured data (simulation not shown). Thus, ADR is a useful, simplified parameter that captures influencing factors other than those captured by the ACV in microsphere entrapment.

Our dichotomous bifurcation model returned HDV values of 20 to 130 cm^3, indicating that our model reflects the final arteriole tree and not the entire hepatic artery tree. In addition, the entrapment of the microspheres was present only in generations 12 and higher, and simulations starting in the-arteriole part of the artery tree (ie, from generation 9) resulted in results similar to those derived from starting the simulation from generation 1. For this reason, our model is useful for small-scale analysis, but macro analysis of microsphere distributions in specific liver segments should include data from imaging methods such as single-photon emission computed tomography or positron emission tomography.

The tolerance of normal liver tissue for resin microspheres is under debate because a variety of administration methods and retrospective dosimetry methods are currently in use (2, 10). Strigari et al (1) reported a 50% probability of complications (serious or fatal radiation-induced symptoms) at a maximal absorbed dose (MAD) of 52 Gy to the entire normal liver parenchyma (73 patients) when the non-individualized and commonly applied body surface area method was applied to determine the amount of activity to be injected. Lau et al (22), who applied the more demanding but personalized partition model (23), identified 0 of 71 patients with complications when the MAD to the total normal liver parenchyma was 25 to 136 Gy (median patient MAD, 52 Gy). In a review article about patient selection for SIRT, Lau et al (24) recommended MADs of <50 Gy to normal liver parenchyma for whole-liver treatments with resin SIR-Spheres and <70 Gy for single-lobe treatments. Kao et al (25) did not observe acute toxicity in 10 patients after applying the same partition model and fulfilling the absorbed dose constraints recommended by Lau et al (24).

Few small-scale dosimetry studies have been performed to complement the performed dosimetry and to investigate the apparently high tolerability for SIRT. Walrand et al (3) used their artery branching tree model to compare the tolerability of glass and resin microspheres. They determined that the fraction of portal tracts receiving an absorbed dose of <40 Gy with glass microspheres at a MAD to the entire liver parenchyma of 120 Gy was similar to the fraction for resin microspheres at a MAD of only 40 Gy (3). For resin microspheres, the MAD was much lower for the central veins and the liver parenchyma, but the portal tract is the critical structure for radioembolization, and the nonuniform distribution of absorbed doses to these structures was suspected to explain the apparently higher tolerance for glass microspheres than for resin microspheres (3). It is notable, however, that most patients treated with resin microspheres who receive a MAD of >40 Gy to

the liver parenchyma still do not manifest acute toxic effects or radioembolization-induced liver disease, even though such complications are evident for external beam radiation therapy at MADs of only 30 to 40 Gy (26).

From a treatment perspective, it is highly valuable to derive more accurate MAD than currently is possible, and further evaluation of the small-scale influence of MAD is essential. Our model reproduces the formation of clusters and their distribution in the artery tree but lacks spatial information, which is required for an accurate small-scale dosimetry. Still, our results indicate how the cluster formation depends on the variability in artery diameters and artery concentration in different parts of the liver, which might be useful for future spatial modeling of microsphere distributions in the whole liver by recent modeling approaches of bifurcation vessel trees (19). The theoretical framework for the most common approaches to determine the artery angle and radii at the bifurcations is by assuming that the metabolic cost for maintaining the artery walls is in balance with the power released from the blood transport (27-29). This assumption leads to the inference that the ratio of the parent artery radii to the sum of the daughter artery radii is a power function with the exponent ranging between 2.55 and 3, depending on the flow and artery properties (19). When calculating the corresponding exponential value for the measured artery tree diameters by Debbaut et al (12), an exponent of 2.24 is achieved. This deviation from the theoretically determined values is most probably due to the polyfurcation in the native artery tree, which, if included, would decrease the value in the theoretical studies. We plan to enhance our modeling with the above-described features and explore the impact of different exponential values and extend this work into a spatial model valuable for detailed small-scale dosimetry.

In conclusion, using human biopsy material, we have characterized microsphere clusters and their locations in different-sized arterioles and have shown that this distribution can be modeled with a novel dichotomous bifurcation model. These results indicate that the microsphere distribution in normal liver parenchyma is highly variable and increases with increasing microsphere concentration, which highlights the need for caution during post-therapeutic analysis of microsphere distributions; currently available noninvasive imaging methods can reveal only macroscopic nonuniformities in activity distributions. Furthermore, the increasing tendency of microspheres to form clusters within higher microsphere concentrations underscores the potential for optimizing microsphere radioembolizations in terms of small-scale and macroscopic absorbed dose distributions in normal liver tissue.

References

1. Strigari L, Sciuto R, Rea S, et al. Efficacy and toxicity related to treatment of hepatocellular carcinoma with 90Y-SIR spheres: Radiobiologic considerations. *J Nucl Med* 2010;51:1377-1385.
2. Chiesa C, Mira M, Maccauro M, et al. Radioembolization of hepatocarcinoma with (90)Y glass microspheres: Development of an individualized treatment planning strategy based on dosimetry and radiobiology. *Eur J Nucl Med Mol Imaging* 2015;42:1718-1738.
3. Walrand S, Hesse M, Chiesa C, et al. The low hepatic toxicity per Gray of 90Y glass microspheres is linked to their transport in the arterial tree favoring a nonuniform trapping as observed in posttherapy PET imaging. *J Nucl Med* 2014;55:135-140.
4. Burton MA, Gray BN, Klemp PF, et al. Selective internal radiation therapy: Distribution of radiation in the liver. *Eur J Cancer Clin Oncol* 1989;25:1487-1491.
5. Högberg J, Rizell M, Hultborn R, et al. Heterogeneity of microsphere distribution in resected liver and tumour tissue following selective intrahepatic radiotherapy. *EJNMMI Research* 2014;4:48.
6. Högberg J, Rizell M, Hultborn R, et al. Increased absorbed liver dose in selective internal radiation therapy (SIRT) correlates with increased sphere-cluster frequency and absorbed dose inhomogeneity. *EJNMMI Physics* 2015;2:10.
7. Fox RA, Klemp PF, Egan G, et al. Dose distribution following selective internal radiation therapy. *Int J Radiat Oncol Biol Phys* 1991;21:463-467.
8. Campbell AM, Bailey IH, Burton MA. Analysis of the distribution of intra-arterial microspheres in human liver following hepatic yttrium-90 microsphere therapy. *Phys Med Biol* 2000;45:1023-1033.
9. Kennedy AS, Nutting C, Coldwell D, et al. Pathologic response and microdosimetry of (90)Y microspheres in man: Review of four explanted whole livers. *Int J Radiat Oncol Biol Phys* 2004;60:1552-1563.
10. Cremonesi M, Chiesa C, Strigari L, et al. Radioembolization of hepatic lesions from a radiobiology and dosimetric perspective. *Front Oncol* 2014;4:210.
11. Kennedy AS, McNeillie P, Dezarn WA, et al. Treatment parameters and outcome in 680 treatments of internal radiation with resin 90Y-microspheres for unresectable hepatic tumors. *Int J Radiat Oncol Biol Phys* 2009;74:1494-1500.
12. Debbaut C, Segers P, Cornillie P, et al. Analyzing the human liver vascular architecture by combining vascular corrosion casting and micro-CT scanning: A feasibility study. *J Anat* 2014;224:509-517.
13. Oda M, Yokomori H, Han JY. Regulatory mechanisms of hepatic microcirculatory hemodynamics: Hepatic arterial system. *Clin Hemorheol Microcirc* 2006;34:11-26.
14. Crawford AR, Lin XZ, Crawford JM. The normal adult human liver biopsy: A quantitative reference standard. *Hepatology* 1998;28:323-331.
15. Rappaport AM. The structural and functional unit in the human liver (liver acinus). *Anat Rec* 1958;130:673-689.
16. Rappaport AM. The microcirculatory hepatic unit. *Microvasc Res* 1973;6:212-228.
17. Lamers WH, Hilberts A, Furt E, et al. Hepatic enzymic zonation: A reevaluation of the concept of the liver acinus. *Hepatology* 1989;10:72-76.
18. Saxena R, Theise ND, Crawford JM. Microanatomy of the human liver—exploring the hidden interfaces. *Hepatology* 1999;30:1339-1346.
19. Schwen LO, Preusser T. Analysis and algorithmic generation of hepatic vascular systems. *Int J Hepatol* 2012;2012:357687.
20. Högberg J, Rizell M, Hultborn R, et al. Radiation exposure during liver surgery after treatment with (90)Y microspheres, evaluated with computer simulations and dosimeter measurements. *J Radiol Prot* 2012;32:439-446.
21. Kennedy AS, Kleinstreuer C, Basciano CA, et al. Computer modeling of yttrium-90-microsphere transport in the hepatic arterial tree to improve clinical outcomes. *Int J Radiat Oncol Biol Phys* 2010;76:631-637.
22. Lau WY, Ho S, Leung TW, et al. Selective internal radiation therapy for nonresectable hepatocellular carcinoma with intraarterial infusion of 90yttrium microspheres. *Int J Radiat Oncol Biol Phys* 1998;40:583-592.

23. Ho S, Lau WY, Leung TW, et al. Partition model for estimating radiation doses from yttrium-90 microspheres in treating hepatic tumours. *Eur J Nucl Med* 1996;23:947-952.
24. Lau WY, Kennedy AS, Kim YH, et al. Patient selection and activity planning guide for selective internal radiotherapy with yttrium-90 resin microspheres. *Int J Radiat Oncol Biol Phys* 2012;82:401-407.
25. Kao YH, Hock Tan AE, Burgmans MC, et al. Image-guided personalized predictive dosimetry by artery-specific SPECT/CT partition modeling for safe and effective 90Y radioembolization. *J Nucl Med* 2012;53:559-566.
26. Fuss M, Salter BJ, Herman TS, et al. External beam radiation therapy for hepatocellular carcinoma: Potential of intensity-modulated and image-guided radiation therapy. *Gastroenterology* 2004;127:S206-S217.
27. Murray CD. The physiological principle of minimum work: I. The vascular system and the cost of blood volume. *Proc Natl Acad Sci U S A* 1926;12:207-214.
28. Zamir M. Optimality principles in arterial branching. *J Theor Biol* 1976;62:227-251.
29. Sherman TF. On connecting large vessels to small. The meaning of Murray's law. *J Gen Physiol* 1981;78:431-453.